Korean J. Chem. Eng., 40(12), 3003-3016 (2023)
DOI: 10.1007/s11814-023-1569-x

pISSN: 0256-1115
eISSN: 1975-7220

Adsorptive removal of congo red and methylene blue dyes from aqueous solutions by *Rumex obtusifolius* roots

Birol Isik†

Department of Chemistry, Faculty of Arts & Sciences, Yildiz Technical University, Esenler, Istanbul, 34220, Turkey
(*Received 4 August 2023 • Revised 23 August 2023 • Accepted 2 September 2023*)

Abstract−*Rumex obtusifolius* roots were utilized within the scope of zero waste. Sorption of methylene blue and congo red dyes from wastewater was carried out. First, surface properties were determined using inverse gas chromatography. By this method, it was found that the surface of *Rumex obtusifolius* roots was acidic (K_D/K_A=0.13). The point of zero charge value of *Rumex obtusifolius* roots was determined as 5.62. Based on these results and selectivity studies, suitable dyes were selected for sorption studies. Experimental design was used for the first time to determine the parametric effects and to improve the process for the highest methylene blue and congo red removal. Optimum conditions such as pH (2-12), concentration (10-50 mg/L), adsorbent amount (0.01 g/50 mL-0.30 g/50 mL), and contact time (0-210 min) were determined for the adsorption process. The Langmuir-2 model provided the best correlation, and q_m values for methylene blue and congo red dyes were determined as 500.00 mg/g and 128.21 mg/g at 298 K. From the kinetic studies, it was found that the sorption process for methylene blue and congo red dyes followed pseudo-second-order kinetics. The effect of NaCl and $CaCl_2$ salts on methylene blue and congo red sorption on *Rumex obtusifolius* roots was evaluated. The adsorption process was found to be endothermic for methylene blue dye (ΔH^o=+19.33 kJ/mol) and exothermic for congo red dye (ΔH^o=−4.99 kJ/mol). The process was found to be spontaneous for both dyes (ΔG^o=−28.10 kJ/mol for methylene blue dye and ΔG^o=−26.14 kJ/mol for congo red dye at 298 K). All findings showed the potential of *Rumex obtusifolius* roots as a model adsorbent for the removal of various organic pollutants from wastewater.

Keywords: Adsorption, *Rumex obtusifolius* Roots, Surface Properties, Methylene Blue, Congo Red

INTRODUCTION

Water pollution has been causing irreversible environmental damage for many years due to globalization and the advancement of science. Wastewater can adversely influence the quality of drinking water and, as a result, the ecological system as a result of growing water overuse in industrial, home, and agricultural settings. Due to the practices in these fields, the water is contaminated with several contaminants, including dyes, heavy metals, radioactive substances, prescription medications, and pesticides, that are dangerous to the health of all living creatures. These pollutants are produced by a variety of industrial processes, including those in the food, paper, textile, automotive, pharmaceutical, and agricultural industries [1-4]. Significant water contamination is caused by dye use, particularly in the textile industry. Based on the use of dyes in various industries, it has been determined that approximately 7×10^5 tons of dyes are discharged into the aquatic environment each year and significantly damage life [5-7]. The biological system is greatly endangered by the release of dyes into aquatic systems, even in very low quantities. When introduced into aqueous media, the majority of these contaminants are hazardous and do not biodegrade. Additionally, by blocking sunlight from penetrating the aquatic habitat, dyes discharged into the aqueous media limit photosynthetic processes [8,9].

Organic dyes in wastewater can be found in different types such as anionic, cationic, and non-ionic depending on the charge [10, 11]. Congo red (CR) is one of the anionic acidic dyes with formula $C_{32}H_{22}N_6Na_2O_6S_2$, highly soluble in aqueous media and thermally stable. It is also highly resistant to light and biodegradation, which has a significant impact on aquatic ecosystems. Organic CR dye is highly toxic and can cause skin and eye irritation, respiratory problems, and blood clots. During metabolism, it is converted to benzidine, which is also carcinogenic [12,13]. Methylene blue (MB) is a toxic cationic dye with the formula $C_{16}H_{18}ClN_3S$ that is widely used in many industries. Short-term acute exposure to MB dye (>7.0 mg/kg) can lead to increased heart rate, shock, vomiting, cyanosis, jaundice, stone formation, and necrosis of human tissue, while long-term exposure poses a high cancer risk [14-16]. Due to their harmful and toxic effects and their non-biodegradability in aqueous media, such organic dyes need to be effectively removed from aqueous solutions.

Aqueous solutions contaminated with organic dyes are often treated using a variety of techniques, including chemical precipitation, membrane filtration, reverse osmosis, ion exchange, photocatalytic degradation, and adsorption. The type and degree of contamination, the amount of wastewater that has to be treated, and the intended level of treatment can all affect which method is most appropriate. However, many of the technologies for treating dye effluent are not appropriate for small-scale enterprises since they involve a large initial financial outlay as well as increasing costs for the chemicals and equipment needed. The removal of organic dyes

†To whom correspondence should be addressed.
E-mail: 19birol91@gmail.com
Copyright by The Korean Institute of Chemical Engineers.

from aqueous media via adsorption is flexible and useful because of its straightforward design, simplicity in use, high efficacy, and low cost. As a result, research is ongoing to create more effective and eco-friendly adsorbents that can improve the efficacy of this approach even more [17-21].

Biomass wastes have almost no commercial value and are often difficult to dispose of. Therefore, using such wastes as adsorbents can increase their economic value and reduce disposal costs [17]. Among these biomass wastes, *Rumex obtusifolius* is one of the most widely distributed and problematic perennial weeds in temperate regions, grasslands, and field agriculture worldwide. *Rumex obtusifolius* belongs to the Polygonaceae family and its structure is rich in compounds such as anthraquinone, steroids, flavonoids, and phenolic acids. It usually grows near meadows, vacant lots, roadsides, ditches, and shorelines. The leaves of the non-sour species of this plant are widely consumed as food in Anatolia. However, the roots of this plant are considered biomass waste and are disordered without being used [22-24]. For this purpose, *Rumex obtusifolius* roots were considered as zero waste and used as an adsorbent in this study.

For a successful adsorption procedure in adsorption research, it is crucial to choose the kind of pollutant to remove from aqueous solutions. Determining the surface characteristics of the chosen adsorbent, particularly its behavior concerning acidity and basicity, is crucial. Inverse gas chromatography (IGC) is an efficient method for determining the acidity-basicity behavior of an adsorbent surface since it is low cost, highly accurate, quick, and simple to use. Simpler techniques, like pH_{pzc}, can also be used to analyze this characteristic of the adsorbent surface. However, the IGC technique is also frequently used to determine surface energy, which is crucial for figuring out and improving the properties of the material, such as binding to different surfaces, adhesion, wetting, and surface coating [25-29].

In this study, the IGC technique was used to examine the surface characteristics of *Rumex obtusifolius* roots at infinite dilution. Using the knowledge from this section as a guide, *Rumex obtusifolius* roots were used to remove certain organic dyes from aqueous solutions. For adsorption studies, the ideal conditions, including pH, contact time, concentration, temperature, and adsorbent dosage, were established. Models for isotherms, kinetics, and thermodynamics were used with the data. Roots of *Rumex obtusifolius* were examined using FTIR-ATR, SEM, BET, pH_{pzc}, and zeta potential analyses to characterize them.

MATERIALS AND METHODS

1. Chemicals and Characterization Techniques

n-Hexane (Hx, M_w: 86.18 g/mol, assay: ≥99.7%), n-heptane (Hp, M_w: 100.20 g/mol, assay: ≥99.0%), ethyl acetate (EA, M_w: 88.11 g/mol, assay: ≥99.8%), acetone (Ace, M_w: 58.08 g/mol, assay: ≥99.8%), dichloromethane (DCM, M_w: 84.93 g/mol, assay: ≥99.8%), tetrahydrofuran (THF, M_w: 72.11 g/mol, assay: ≥99.8%), and chloroform (TCM, M_w: 119.38 g/mol, assay: ≥99.8%) were purchased from Supelco. Hydrochloric acid (HCl, M_w: 36.46 g/mol, assay: 37.0%) and sodium hydroxide (NaOH, M_w: 40.00 g/mol, assay: ≥95.0%) were acquired from Merck. n-Octane (O, M_w: 114.23 g/mol, assay: ≥99.0%), n-nonane (N, M_w: 128.26 g/mol, assay: ≥99.0%), n-decan (D, M_w: 142.28 g/mol, assay: ≥94.0%), diethyl ether (DEE, M_w: 74.12 g/mol, ≥97.5%), methylene blue (MB, $C_{16}H_{18}ClN_3S$, M_w: 319.85 g/mol, assay: ≥82.0%), congo red (CR, $C_{32}H_{22}N_6Na_2O_6S_2$, M_w: 696.66 g/mol, assay: ≥35.0%), and sodium nitrate ($NaNO_3$, M_w: 84.99 g/mol, assay: ≥99.0%) were purchased from Sigma Aldrich. All chemicals have an extremely high purity.

Agilent Technologies 6890N gas chromatography device was used to investigate the surface properties of *Rumex obtusifolius* roots by IGC technique at infinite dilution. The temperature of the sample injection unit and detector of the gas chromatography device used throughout the studies is 523 K. Nicolet IS10 Thermo Fourier transform infrared-attenuated total reflectance (FTIR-ATR) spectrophotometer device was used to examine the surface functional groups of the *Rumex obtusifolius* roots, conducted in the wavenumber range of 4,000-600 cm^{-1}. The surface morphology of *Rumex obtusifolius* roots was examined by using Zeiss EVO LS10 scanning electron microscopy (SEM) device. The specific surface area and pore size distribution of the *Rumex obtusifolius* roots were examined by Quantachrome Instruments BET analyzer. The surface charge and zeta potential analyses were performed by the Malvern Zeta sizer device. To adjust the solution pH and determine the pH_{pzc} value, Ohaus Starter 3100 pH meter was used.

2. Preparation of Adsorbent and Chromatographic Column

Rumex obtusifolius roots were collected from a forest in Kesan (Yayla), Edirne. The roots were properly washed in water to remove all dirt and contaminants before being dried at room temperature. Following this procedure, the roots were repeatedly boiled in distilled water to get rid of any remaining oil, impurities, proteins, and color. The dried roots were divided into tiny bits and put through a grinder until the particles were between 80 and 100 mesh. The powdered *Rumex obtusifolius* roots were dried for 24 h at 363 K in a vacuum oven. For IGC and adsorption tests, the roots were then kept in a desiccator. A schematic representation of *Rumex obtusifolius* roots is shown in Fig. S1.

Powdered *Rumex obtusifolius* roots were filled into a stainless-steel column about 0.5 meters long. Column ends were plugged with silanized glass wool to prevent loss of material during analysis. For IGC tests, the column was attached to the instrument and conditioned at 403 K for 24 h. Following this procedure, the surface characteristics of *Rumex obtusifolius* roots were assessed using the IGC method at temperatures between 303.2 and 328.2 K.

3. Inverse Gas Chromatography Studies

The chromatographic column was purchased from Alltech Associates Inc. Inert Helium gas was used at a flow rate of 3.7 mL/min for solvent entrainment across the column. IGC tests were conducted in the temperature range 303.2 to 328.2 K with 5-degree temperature increases. Each experiment was conducted at least four times to guarantee the consistency of the data. The IGC instrument was filled with air and organic solvents using a 1 and 10 μL Hamilton syringe. For infinite dilution, the probe (0.1 μL) was taken into the syringe and flushed into the air. Then, the retention times for the probe and air were determined. At least four consecutive injections were made for each probe and air at each set of measurements.

4. Batch Sorption Studies

The elimination of MB and CR dyes from aqueous solutions

was investigated using batch sorption assays. For these tests, the adsorbent was added to 50 mL of dye solution in 100 mL conical flasks, and the water bath was heated and shaken. Batch sorption experiments were carried out at temperatures of 298, 308, and 318 K. Stock solutions of MB and CR dyes were prepared by dissolving accurately and precisely weighed MB and CR dye powders in distilled water at a concentration of 1,000 mg/L. The concentration range for sorption studies was chosen as 10-50 mg/L and these concentrations were prepared by dilution from the stock solution. The agitation speed was kept constant at 150 rpm for sorption tests. Sorption experiments were also performed at different initial pH ranges from 2 to 12. The solution pH was adjusted using 0.1 M NaOH and 0.1 M HCl solutions. The supernatant solution obtained from all batch sorption studies was analyzed by UV-vis spectrophotometer (Shimadzu UV2600) at wavelengths of 663 and 498 nm for MB and CR dyes, respectively. The sorption yield (Yield (%)) and sorption capacity at "t" time (q_t, mg/g) and equilibrium (q_e, mg/g) were calculated using Eqs. (S9), (S10), and (S11), respectively [30-32].

RESULTS AND DISCUSSION

1. Characterization of *Rumex obtusifolius* Roots

The FT-IR spectra of *Rumex obtusifolius* roots before and after MB and CR sorption are shown in Fig. 1. FT-IR spectra provide information about functional groups that may play an active role in the binding of dye molecules to the *Rumex obtusifolius* roots surface. From the spectrum of the sample before sorption, the peaks observed at 3,320, 1,616, 1,241, and 1,016 cm^{-1} correspond to the -OH stretchings, C=O stretchings, S=O sulfur-containing groups, and C-O stretchings, respectively [33]. From the sample after the sorption processes, peak shifting was observed in both dyes. These shifts were attributed to the electrostatic interactions between the surface functional groups of the *Rumex obtusifolius* roots and dye molecules. These shifts clearly show that the hydroxyl, carboxyl, and sulfate groups on the surface of *Rumex obtusifolius* roots acted as

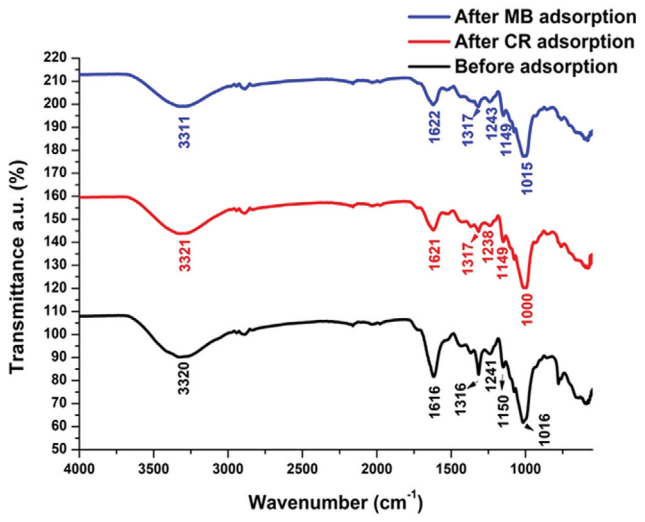

Fig. 1. The FT-IR spectra of *Rumex obtusifolius* roots before and after MB and CR sorption.

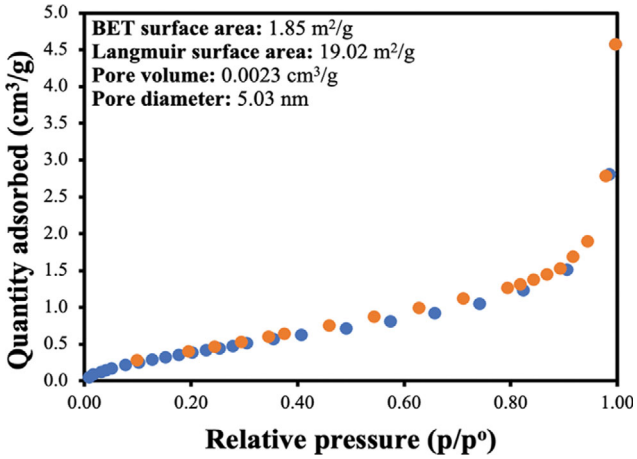

Fig. 2. The N_2 adsorption-desorption isotherms of *Rumex obtusifolius* roots.

active sorption sites during the sorption process.

N_2 adsorption-desorption isotherm curves for *Rumex obtusifolius* roots were shown in Fig. 2. As seen in Fig. 2, the pore volume, average pore diameter, and surface area of *Rumex obtusifolius* roots were determined as 0.0023 cm^3/g, 5.03 nm, and 1.85 m^2/g, respectively, from the BET analysis. According to the IUPAC standard [34], the average pore diameter (5.03 nm) indicates that *Rumex obtusifolius* roots have a mesoporous structure. When the isotherm curves of *Rumex obtusifolius* roots were examined, it was determined that a Type-III isotherm curve appeared. Besides, the isotherm curves show the H3 hysteresis loop. In this case, it can be said that the pores on the surface of *Rumex obtusifolius* roots are parallel-shaped pores [35-37]. The surface area was also calculated as 19.02 m^2/g from Langmuir isotherm. Since the Langmuir isotherm model predicts monolayer adsorption, adsorbate molecules are adsorbed on the surface as a single layer and the surface area is high. On the contrary, since BET isotherm predicts a multilayer adsorption model, adsorbate molecules are distributed in different layers and the surface area decreases [32,38,39].

To investigate the morphological characteristics of *Rumex obtusifolius* roots, SEM analysis was performed and the results shown in Fig. 3 before and after sorption. Fig. 3(a) shows the SEM images of *Rumex obtusifolius* roots before sorption and Fig. 3(b) and (c) show the SEM images after sorption of MB and CR dye, respectively. As seen in Fig. 3, *Rumex obtusifolius* roots have a compact surface due to the appearance of amorphous lignin, hemicellulose, and other non-cellulosic components. Furthermore, *Rumex obtusifolius* roots were found to have a fibrous and rough structure. *Rumex obtusifolius* roots have a rough, porous, and heterogeneous surface structure that allows MB and CR ions to bind to the surface of the fibers [40].

Rumex obtusifolius roots were tested for pH_{pzc} using the salt addition method. 50 mL (0.1 M) of sodium nitrate solution was combined with 0.2 g of *Rumex obtusifolius* roots at an initial pH (pH_i) range of 2 to 12. The solution at different pH was put in a shaker for 48 h at 298 K to determine the final pH (pH_f). The pH_{pzc} was analyzed using ΔpH ($pH_f - pH_i$) versus pH_i plot for *Rumex obtusifolius* roots [41,42]. The determination of the pH_{pzc} value of *Rumex*

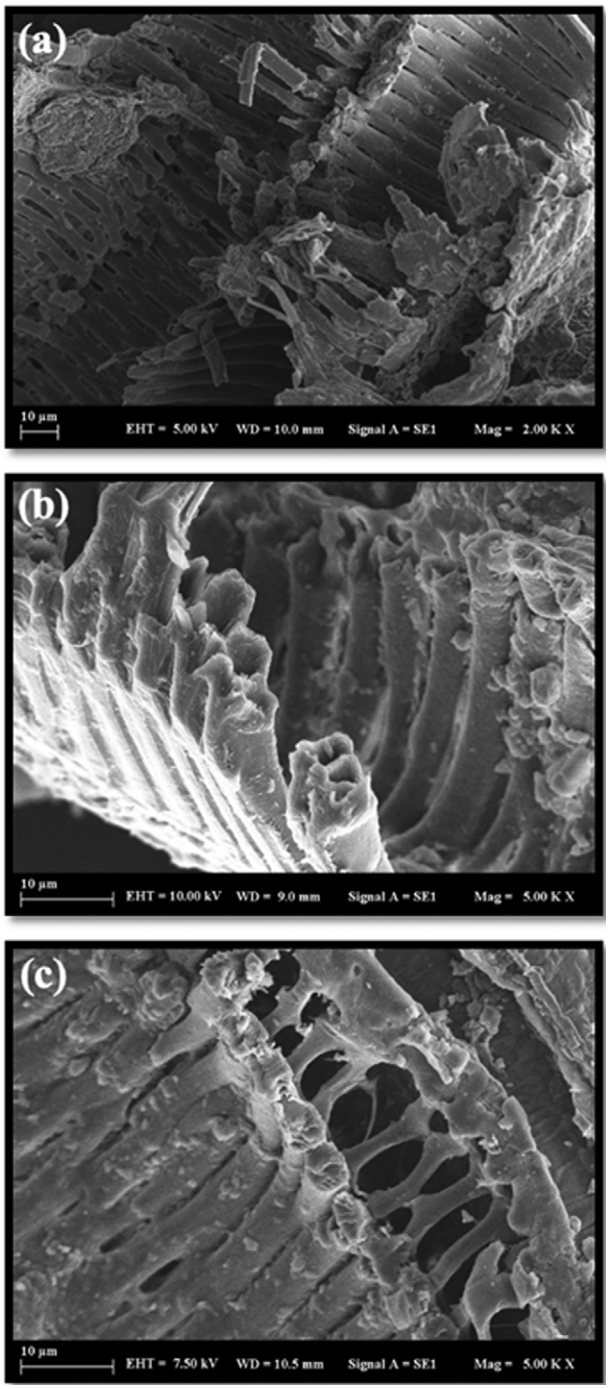

Fig. 3. The SEM images of *Rumex obtusifolius* roots before (a) and after MB (b) and CR (c) adsorption.

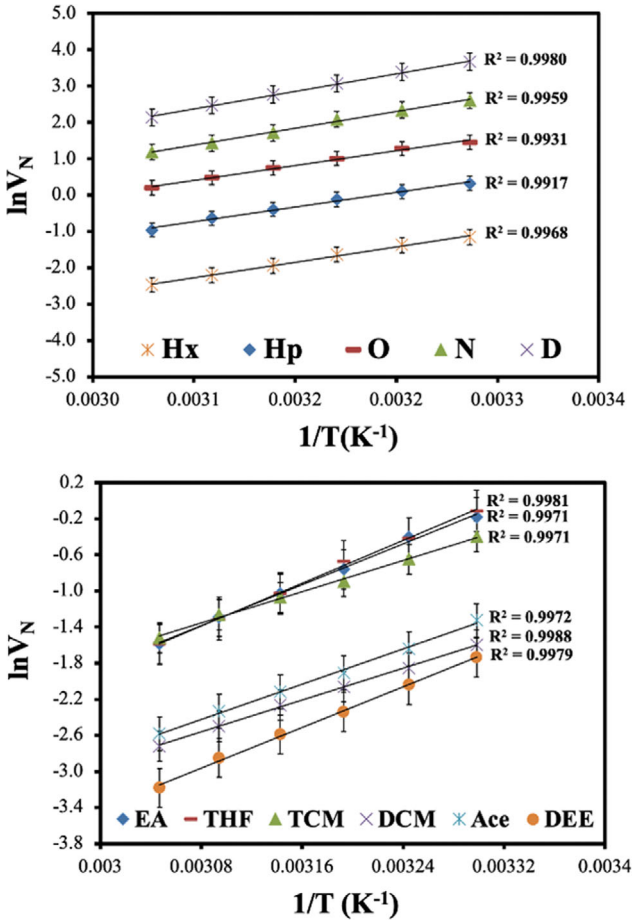

Fig. 4. The retention diagrams for non-polar (Hx, Hp, O, N, and D) and polar solvents (EA, THF, TCM, DCM, Ace, and DEE) on *Rumex obtusifolius* roots.

obtusifolius roots is very important for determining the pH point at which the surface is neutral in terms of electrostatic charges. The pH_{pzc} value of *Rumex obtusifolius* roots was determined as 5.62 as shown in Fig. S2. The surface of *Rumex obtusifolius* roots is positively charged below the pH_{pzc} value and enables the sorption of anionic species, while above the pH_{pzc} value it is negatively charged and enables the sorption of cationic species [43]. Fig. S2 provides the zeta potential analysis of *Rumex obtusifolius* roots at neutral pH. The research revealed that *Rumex obtusifolius* roots have a zeta potential of –21.90 mV, which is consistent with the presence of negative charges on the sample's surface and is advantageous for the sorption of cationic dyes [44].

2. Surface Properties of *Rumex obtusifolius* Roots

The surface properties of *Rumex obtusifolius* roots were investigated with the help of retention times obtained as a result of the interactions between the active sorption sites on the surface of the *Rumex obtusifolius* roots and solvent molecules and net retention volumes (V_N) calculated according to Eq. (S1) [45,46]. Linear retention diagrams of $\ln V_N$ versus 1/T according to Eq. (S1) were plotted and shown in Fig. 4. Surface properties of *Rumex obtusifolius* roots were calculated with the data obtained from these diagrams.

The mechanism of interaction between n-alkanes and *Rumex obtusifolius* roots is the dispersion force, which is important for the investigation of the dispersive surface energy (γ_S^D) of this biomass waste. This value arises as a result of weak interactions such as London, van der Waals, and hydrogen bonds on the surface of *Rumex obtusifolius* roots. The γ_S^D value was calculated according to the Dorris-Gray, Schultz, and Donnet-Park approaches whose linear equations are given in the supporting information file [47-49].

According to the Dorris-Gray method, the γ_S^D value was calcu-

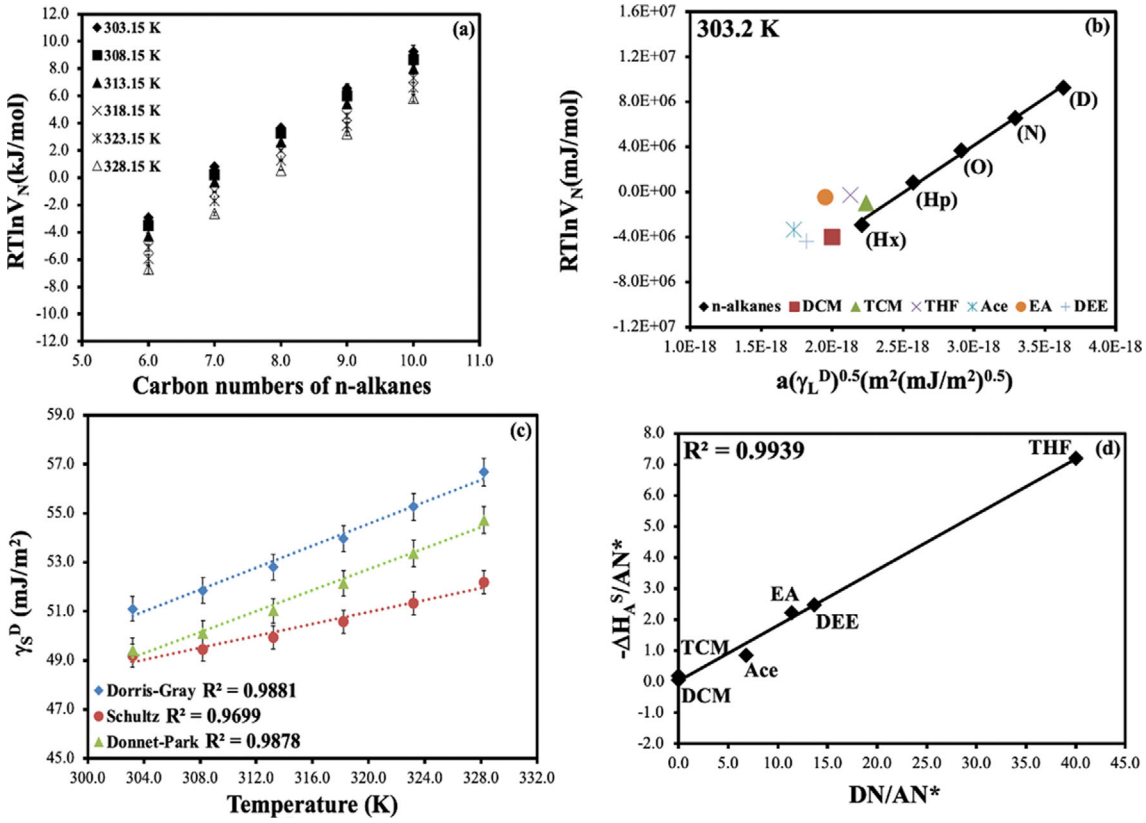

Fig. 5. The linear plots of IGC results: (a) The linear plots of $RTlnV_N$ vs. carbon numbers of n-alkanes, (b) The linear Schultz plots in 303.2 K, (c) The variation of the γ_S^D value vs. temperature for a different method, and (d) The linear plot of $-\Delta H_A^S/AN^*$ vs. DN/AN^*.

lated by substituting $\Delta G_{[CH_2]}$ values obtained from the slope of the linear graph (Fig. 5(a)) plotted between the $RTlnV_N$ values versus the carbon number of n-alkanes according to. Eq. (S6), γ_{CH_2} values calculated according to Eq. (S4), and a_{CH_2} values taken from the literature in Eq. (S3) and all results are presented in Table S1. According to the Donnet-Park approach, the γ_S^D value is calculated similarly to the Dorris-Gray approach. The only difference between the two approaches is the calculation of γ_{CH_2} values. According to the Dorris-Gray approach, the γ_{CH_2} value is calculated by Eq. (S4), while according to the Donnet-Park approach, this value is calculated by Eq. (S5). The γ_S^D values calculated from these approaches are presented in Table S1. As seen in Table S1, the γ_S^D values increase with temperature. It was determined that a stronger binding takes place on the *Rumex obtusifolius* roots surface at higher temperatures and higher energy is required at higher temperatures to remove the bound molecules from the surface.

The γ_S^D value was also calculated according to the Schultz method from the slope of the linear plot of $RTln(V_N)$ versus $a(\gamma_S^D)^{0.5}$ values given in Fig. 5(b) according to Eq. (S7) and the results are presented in Table S1. As seen in Table S1, similar to the other approaches, the γ_S^D values increase with temperature in the Schultz approach. The γ_S^D values were determined as 51.10-56.68 mJ/m^2 for the Dorris-Gray approach, 49.41-54.72 mJ/m^2 for the Donnet-Park approach, and 49.19-52.19 mJ/m^2 for the Schultz approach, respectively. Similar results have been obtained in studies in the literature [50,51].

The three approaches for the calculation of the γ_S^D values were compared and it was found that all three approaches show a linear change with temperature, and the results are shown in Fig. 5(c). As seen from Fig. 5(c), the Dorris-Gray method was found to have a higher correlation coefficient (R^2=0.9881).

Sorption Gibbs free energy (ΔG_A) values for polar solvents can be calculated from the linear plots of the Schultz approach. In the plot in Fig. 5(b), ΔG_A values were calculated from the vertical distances of the symbols of polar solvents to the linear line of n-alkanes. The results are presented in Table 1, where positive ΔG_A values indicate that the sorption process of polar solvents on *Rumex obtusifolius* roots is non-spontaneous.

Table 2 shows the sorption enthalpy (ΔH_A) values of polar solvents on *Rumex obtusifolius* roots. According to Table 2, there is an

Table 1. The variation of ΔG_A (kJ/mol) between *Rumex obtusifolius* roots and the polar solvents

T (K)	EA	Ace	DCM	TCM	THF	DEE
303.2	4.28	3.25	0.29	1.30	2.93	1.46
308.2	4.26	2.96	0.12	1.18	2.70	1.17
313.2	3.99	2.88	0.18	1.19	2.69	0.98
318.2	4.07	3.08	0.37	1.48	2.53	1.04
323.2	4.10	3.19	0.42	1.67	2.47	1.03
328.2	3.23	2.41	−0.29	0.92	1.68	−0.01

Table 2. $-\Delta H_A$ values for the polar solvents onto *Rumex obtusifolius* roots

Polar solvents	Ace	EA	THF	DCM	TCM	DEE
ΔH_A (kJ/mol)	8.84	13.97	15.11	3.26	1.37	14.58

order between the $-\Delta H_A$ values as follows: THF>DEE>EA>Ace>DCM>TCM. According to this order, THF interacts better with the acidic *Rumex obtusifolius* roots surface because it is a basic solvent, while TCM is an acidic solvent and interacts weaker with the acidic *Rumex obtusifolius* roots surface. Additionally, the ΔH_A values illustrate that the sorption process onto *Rumex obtusifolius* roots takes place exothermically.

The acidity-basicity behavior of the *Rumex obtusifolius* roots surface was calculated by Eq. (S8) using the $-\Delta H_A$ values in Table 2 and Gutmann's donor and acceptor numbers. Lewis acid and base constants were utilized to determine the acidity or basicity of the adsorbent surface, and the results were used to forecast the sort of pollutant that would be adsorbed from aqueous media [52,53]. Fig. 5(d) shows the linear plot of $-\Delta H_A^S/AN^*$ vs. DN/AN^*. The acidity (K_A) and basicity (K_D) constants of the *Rumex obtusifolius* roots surface were calculated from the slope and intercept of this linear plot. Accordingly, the K_A value for the *Rumex obtusifolius* roots surface was calculated as 0.1788 and the K_D value as 0.0231. The K_D/K_A value obtained by the ratio of these two values was calculated as 0.13. Since this value is less than 1, it can be said that the *Rumex obtusifolius* roots surface has an acidic character, anionic functional groups can be found on its surface and it can be used as a suitable adsorbent for removing cationic pollutants.

3. Selectivity Tests

To investigate the selective sorption of toxic organic dyes on *Rumex obtusifolius* roots, 0.1 g of *Rumex obtusifolius* roots was added to 50 mL aqueous solutions containing organic dyes (methylene blue, methyl orange, safranine T, malachite green, rhodamine B, congo red, crystal violet, alizarin red S, and indigo carmine) with dye concentrations of 20 mg/L. The mixtures were stirred in a water bath with a heater and shaker at 150 rpm for the contact time (90 min). The supernatant solutions were then analyzed by UV-vis spectrophotometry after centrifugation at 9,000 rpm. The sorption yield

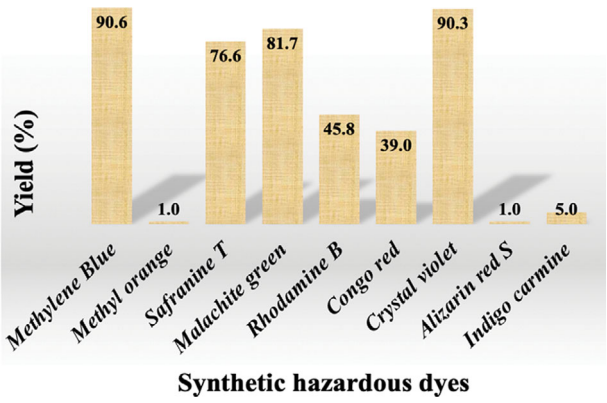

Fig. 6. The selectivity of different cationic and anionic dyes onto *Rumex obtusifolius* roots.

was calculated by Eq. (S9) using the data obtained here and the results shown as column graphs in Fig. 6. As seen in Fig. 6, it was observed that anionic dyes were not absorbed very well on the *Rumex obtusifolius* roots, while cationic dyes were adsorbed better. When the dye sorption yields were ranked, they followed the following order: Methylene blue>Crystal violet>Malachite green>Safranine T>Rhodamine B>Congo red>Indigo carmine>Methyl orange= Alizarin red S. According to these results, MB (90.6%) and CR (39.0%) dyes, which have the highest sorption yield among anionic and cationic dyes, were selected as model dyes in this work.

4. Optimum Conditions for Sorption Studies

4-1. Influence of *Rumex obtusifolius* Roots Dosage

The adsorbent dosage is one of the important conditions affecting the sorption process of organic dyes. Fig. 7(a) shows the effect of the dosage of *Rumex obtusifolius* roots on the sorption of both MB and CR dyes. As seen in Fig. 7(a), it was determined that the sorption capacity (q_e) decreased as the dosage of *Rumex obtusifolius* roots increased, whereas the sorption yield increased. For MB sorption, the sorption yield increased rapidly by increasing the dosage of *Rumex obtusifolius* roots from 0.01 g/50 mL to 0.05 g/50 mL. However, further increasing the dosage of *Rumex obtusifolius* roots increased the sorption yield very little and it remained almost constant at 99.0%. For the sorption of CR dye, the sorption yield increased continuously with increasing *Rumex obtusifolius* roots dosage up to 0.30 g/50 mL and reached approximately 69.0% at 0.30 g/50 mL. This increasing trend in the sorption yield of both dyes is the result of the expansion of the surface area with the increase in the dosage of *Rumex obtusifolius* roots and the emergence of more active sorption sites [54-56]. The sorption yield gradually decreased with the increase in the dosage of *Rumex obtusifolius* roots. This trend is due to the possibility of interactions between adsorbent particles (aggregation or agglomeration) with increasing *Rumex obtusifolius* roots dosage, which reduces the total surface area.

4-2. Influence of Initial pH

The solution pH is an extremely important parameter for the functioning and performance of the sorption process of MB and CR dyes on *Rumex obtusifolius* roots. To investigate the effect of solution pH, MB and CR dye solutions (20 mg/L concentration) were prepared and the pH was varied from 2 to 12 for both dye types. Fig. 7(b) shows the effect of solution pH on the sorption of MB and CR dyes on *Rumex obtusifolius* roots. As seen in Fig. 7(b), the solution pH significantly affected the sorption process of both dyes, because the change in solution pH can affect the degree of ionization of easily protonated and deprotonated functional groups. The sorption yield of cationic MB dye on *Rumex obtusifolius* roots was significantly lower at acidic pH values ($pH<pH_{pzc}$: 5.62), while the sorption yield of anionic CR dye was higher at acidic pH values ($pH<pH_{pzc}$: 5.62). This is since at acidic pH values ($pH<pH_{pzc}$: 5.62), the anionic CR dye adsorbs more, and the cationic MB dye adsorbs less because the *Rumex obtusifolius* roots surface is rich in positive charge (H^+) [57-59]. On the other hand, at basic pH values ($pH>pH_{pzc}$: 5.62), since the *Rumex obtusifolius* roots surface will be richer in negative charges, the sorption yield of the cationic MB dye was found to increase, while the sorption yield of the anionic CR dye decreased. The optimum pH value for both dyes was determined as approximately 7 to reduce both the pH range of textile

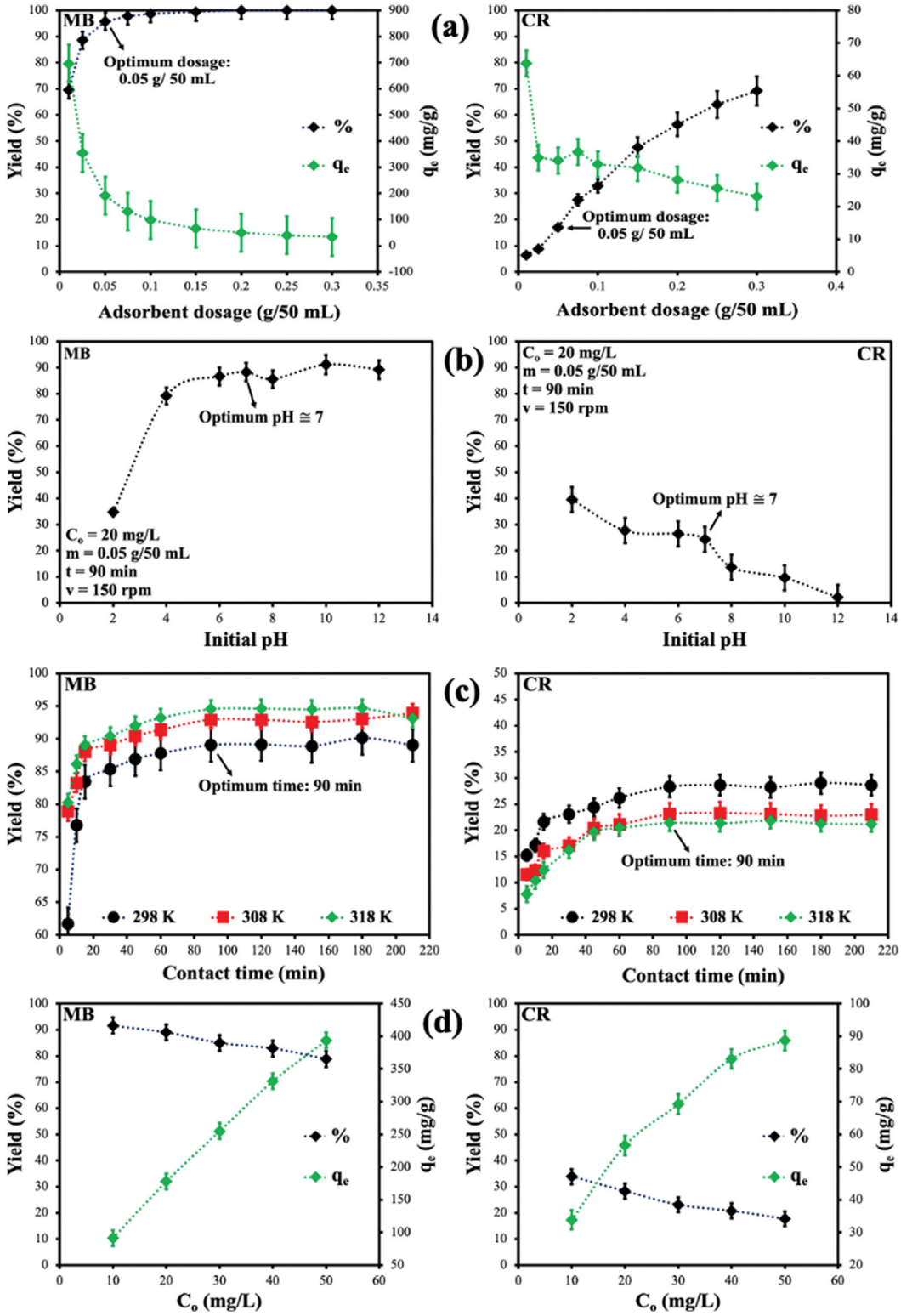

Fig. 7. The optimum physicochemical parameters of sorption of MB and CR dyes onto *Rumex obtusifolius* roots: (a) adsorbent dosage, (b) initial pH, (c) contact time, and (d) initial concentration.

dyes in aqueous solutions (6-10) and the cost.

4-3. Influence of Contact Time

Fig. 7(c) illustrates the effect of contact time on the sorption process of MB and CR dyes on *Rumex obtusifolius* roots at 20 mg/L initial concentration, pH=7, 0.05 g/50 mL adsorbent dosage. As seen in Fig. 7(c), the sorption yield reached 90.0% in the first 20 min of the sorption process for MB dye with increasing contact time. The sorption yield increased slowly until 90 min contact time reached

95.0% and remained almost constant after 90 min. Similarly, for CR dye, the sorption yield reached 25.0% in the first 20 min of the sorption process. The sorption efficiency increased slowly until 90 min contact time, reaching 30.0%, and remained almost constant after 90 min. According to these results, the contact time was determined as 90 min for both dyes. These trends in sorption yields are because the active sorption sites are empty at the initial stage of the sorption process and gradually fill as the process progresses [60-62]. As seen from Fig. 7(c), the sorption yield increases with increasing temperature for MB dye, while it decreases with increasing temperature for CR dye. In this case, the sorption process is endothermic for MB dye and exothermic for CR dye.

4-4. Influence of Initial Concentration

Fig. 7(d) shows the effect of initial MB and CR concentrations (10-50 mg/L) on the sorption process. In Fig. 7(d), it is seen that the sorption yields of MB and CR dye molecules decrease with an increase in concentration. While the sorption yields for MB and CR dyes are 91.63% and 33.87% at 10 mg/L, they decrease to 78.76% and 17.74% at 50 mg/L, respectively. This trend is due to the presence of more active sorption sites for dye sorption on the *Rumex obtusifolius* roots surface at lower dye concentrations. However, at higher dye concentrations, the sorption yield decreases as the active sorption sites become saturated with dye molecules. On the other hand, with increasing initial concentration, the sorption efficiency by *Rumex obtusifolius* roots increase due to the driving force to overcome the mass transfer resistance between the bulk liquid phases and the solid phase, revealing a significant potential for MB and CR dyes [63-65].

4-5. Influence of Ionic Strength

Fig. 8 shows the effect of NaCl and $CaCl_2$ salts on the MB and CR sorption process on *Rumex obtusifolius* roots. A decrease for MB dye and an increase for CR dye in sorption yield was observed when NaCl and $CaCl_2$ were added to the solution. For MB sorption, the sorption yield decreased from 85.2% to 65.1% with the addition of NaCl, while it decreased from 85.2% to 55.6% with the addition of $CaCl_2$. On the other hand, CR sorption, increased from 32.7% to 79.7% with the addition of NaCl, while it increased from 32.7% to 83.1% with the addition of $CaCl_2$. The decrease in MB dye is due to the inhibition of the active sorption sites of the *Rumex obtusifolius* roots surface by NaCl and $CaCl_2$ salts. Na^+ and Ca^{2+} ions are thought to interfere with the interactions between the positively charged MB molecules and the negatively charged parts of the *Rumex obtusifolius* roots surface. On the other hand, these ions turn the negative parts of the *Rumex obtusifolius* roots surface into positive active sorption sites and lead to an increase in the sorption yield for the anionic CR dye [66,67].

5. Sorption Equilibrium Studies

Langmuir, Freundlich, and D-R isotherms were applied to determine the relationship between the amount of MB and CR dyes adsorbed per gram of *Rumex obtusifolius* roots and the concentration of MB and CR ions in equilibrium [68,69]. Isotherm curves for MB and CR dyes are shown in Fig. S3(a). As seen in Fig. S3(a), it was observed that the sorption process of both MB and CR dyes on *Rumex obtusifolius* roots followed the L-2 type isotherm model according to Giles' classification. The linear equations of the four types of Langmuir isotherm, Freundlich isotherm, and D-R isotherm are listed in Table S2.

The Langmuir isotherm is the simplest theoretical representation of monolayer sorption on a surface with finitely many identical sites. This model indicates that the sorption process occurs at certain homogeneous sites inside the adsorbent, i.e., once a dye molecule occupies a site on the adsorbent surface, no additional

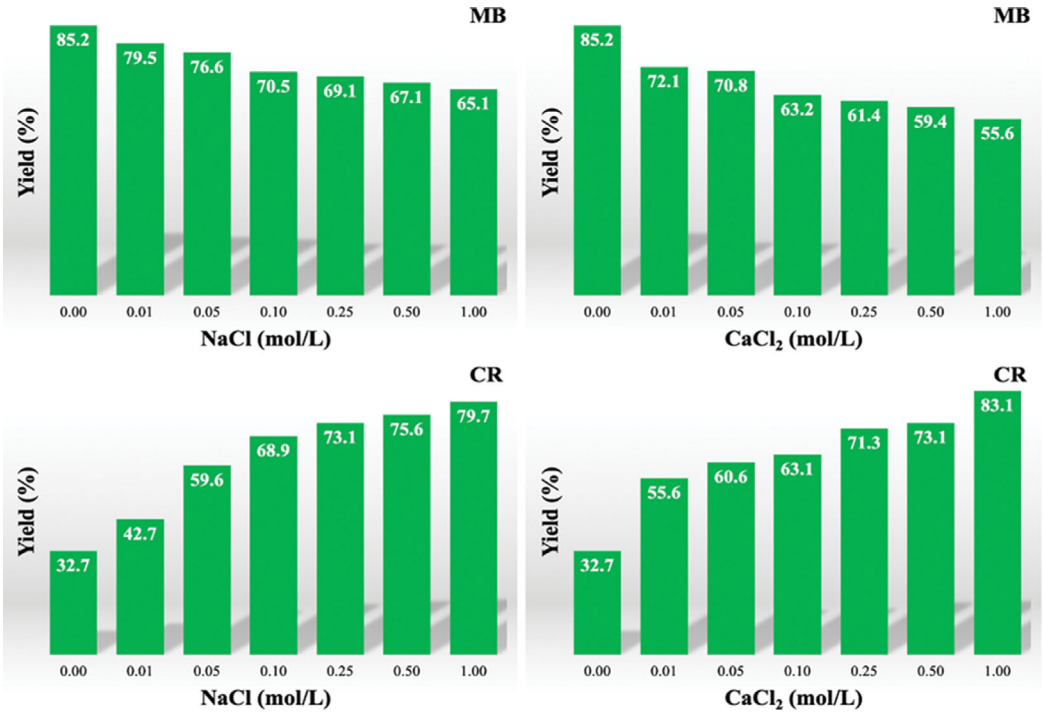

Fig. 8. Effect of ionic strength on MB and CR sorption yield of *Rumex obtusifolius* roots.

Table 3. Isotherm parameters for the sorption of MB and CR dyes on *Rumex obtusifolius* roots

	Rumex obtusifolius roots					
	MB			CR		
Temp. (K)	298	308	318	298	308	318
Langmuir-1						
q_m (mg/g)	555.56	555.56	588.24	129.87	101.01	87.72
K_L (L/mg)	0.2143	0.3333	0.4146	0.0530	0.0580	0.0580
r^2	0.9889	0.9981	0.9955	0.9959	0.9882	0.9910
Langmuir-2						
q_m (mg/g)	500.00	555.56	588.24	128.21	105.26	96.15
K_L (L/mg)	0.2667	0.3333	0.4359	0.0542	0.0530	0.0477
r^2	0.9971	0.9990	0.9997	0.9987	0.9960	0.9949
Langmuir-3						
q_m (mg/g)	520.14	548.95	587.12	128.77	103.84	91.54
K_L (L/mg)	0.2464	0.3454	0.4338	0.0540	0.0546	0.0530
r^2	0.9608	0.9913	0.9899	0.9870	0.9603	0.9584
Langmuir-4						
q_m (mg/g)	531.18	551.46	590.41	129.48	105.93	93.42
K_L (L/mg)	0.2367	0.3424	0.4294	0.0533	0.0524	0.0507
r^2	0.9608	0.9913	0.9899	0.9870	0.9603	0.9584
Freundlich						
K_F (mg/g) $(L/g)^{1/n}$	106.38	137.74	165.75	12.91	10.94	9.48
1/n	0.5759	0.5568	0.5761	0.5323	0.5174	0.5180
r^2	0.9928	0.9732	0.9834	0.9857	0.9684	0.9568
Dubinin-Radushkevich (D-R)						
$q_{D\text{-}R}$ (mg/g)	314.54	345.54	362.38	80.92	67.00	59.55
$E_{D\text{-}R}$ (kJ/mol)	1.21	1.50	1.86	0.26	0.25	0.25
r^2	0.8801	0.9257	0.9200	0.9199	0.9270	0.9631

sorption occurs at that site. The Langmuir model has four linear forms [70,71]. The equations of these linear forms are given in Table S2. The experimental data were applied to the four types of Langmuir models given in Eqs. (S12), (S13), (S14), and (S15), respectively, and the results are in Table 3. As seen in Table 3, among the correlation coefficients of the four types, the Langmuir-2 type was found to have a higher correlation than the others. Therefore, only the linear graphs of the Langmuir-2 type are shown in Fig. S3(b). The q_m values calculated from the Langmuir-2 model were determined as 500.00 mg/g and 128.21 mg/g for MB and CR dyes at 298 K, respectively. The high q_m values show that *Rumex obtusifolius* roots are an effective adsorbent. As seen from these results, since the *Rumex obtusifolius* roots surface has acidic and anionic functional groups, cationic MB dye is adsorbed more while anionic CR dye is adsorbed less. Similar results were obtained in other Langmuir types. The K_L isotherm constants obtained from the Langmuir-2 model were in the range of 0-1, indicating that the sorption process was favorable [72]. These values were used to calculate the thermodynamic equilibrium constant. Additionally, with increasing temperature, the q_m value of MB dye increased from 500.00 mg/g to 588.24 mg/g, while that of CR dye decreased from 128.21 mg/g to 96.15 mg/g. These results indicate that the MB sorption process on *Rumex obtusifolius* roots was endothermic while the CR sorption process was exothermic. To compare the removal efficiency of *Rumex obtusifolius* roots for various pollutants from aqueous solutions and to determine its effectiveness, the q_m values were compared with studies in the literature and listed in Table 4.

The Freundlich isotherm describes the chemical adsorption of low-concentration solutions on heterogeneous layers by the interaction of adsorbed molecules distributed by heat and energy with high adsorption capacity [76,77]. According to Eq. (S16) in Table S2, a linear plot of $\ln q_e$ versus $\ln C_e$ was plotted and shown in Fig. S3(c). The isotherm parameters calculated from the slope and intercept of this plot are listed in Table 3. As seen in Table 3, the "1/n" value for both dyes ranges between 0.5-0.6, indicating that the sorption process is favorable for both dyes. When the correlation coefficients are analyzed, it is seen that they are lower compared to the Langmuir isotherm, which is an indication that the sorption process takes place on monolayer and homogeneous surfaces.

With a Gaussian surface distribution on a heterogeneous surface, the D-R isotherm serves as an empirical model to describe the mechanism of sorption. The pore-filling mechanism is followed by a

Table 4. The comparison of sorption properties of the agricultural waste in this study and with literature data

Agricultural waste	Temp. (K)	Dye	q_m (mg/g)	Ref.
Rumex obtusifolius roots	298	MB	500.00	This work
Rumex obtusifolius roots	298	CR	128.21	This work
Labada (*Rumex*) biowaste	298	RhB	104.91	[33]
Citrus limetta peel waste	298	MB	227.30	[73]
Black cardamom activated carbon	298	CR	69.93	[74]
Ashitaba waste activated carbon	298	CR	345.17	[75]
Walnut shell activated carbon	298	MB	314.19	[75]

semi-empirical equation in this model. Presumably, a multiplayer character participates in the physical sorption process by using van der Waal's forces. It depends on the temperature of the D-R isotherm [78,79]. Linear plots of $\ln q_e$ versus ε^2 were plotted according to Eq. (S17) in Table S2 and shown in Fig. S3(d). Isotherm parameters were calculated from the slope and intercept of these plots and listed in Table 3. Using the b values calculated from the slope, $E_{D\text{-}R}$ values were calculated using the "$E_{D\text{-}R}=1/(-2\beta)^{0.5}$" equation and listed in Table 3. If the $E_{D\text{-}R}$ values are less than 8 kJ/mol, the sorption is physical; if it is between 8-16 kJ/mol, it is ionic; and if it is greater than 16 kJ/mol, it is chemical [80]. As seen in Table 3, since the $E_{D\text{-}R}$ values are less than 8 kJ/mol for both dyes, it can be said that the sorption of MB and CR dyes on *Rumex obtusifolius* roots is physical. However, the low correlation coefficients are insufficient to explain that the sorption process occurs physically.

6. Sorption Kinetic Studies

The kinetic behavior of MB and CR dye sorption by *Rumex obtusifolius* roots was examined using pseudo-first-order (PFO), pseudo-second-order (PSO), and intraparticle diffusion (IPD) models [81]. The linear equations for these kinetic models are listed in Table S2. The linear plots drawn according to Eqs. (S18), (S19), and (S20) in Table S2 are shown in Fig. S4. Kinetic parameters were calculated from the slope and intercept points of the linear plots in Fig. S4 and the results are shown in Table 5. As seen in Table 5, the sorption of MB and CR on *Rumex obtusifolius* roots follows the PSO kinetic due to the high correlation coefficients. Moreover, experimental and calculated q_e values also support that the sorption process follows the PSO model. While these values are quite close to each other in the PSO model, the values are quite different in the PFO model.

Table 5. Kinetic parameters for the sorption of MB and CR dyes on *Rumex obtusifolius* roots

	Rumex obtusifolius roots					
	MB			CR		
Temp. (K)	298	308	318	298	308	318
PFO						
k_1 (min^{-1})	0.0495	0.0362	0.0382	0.0304	0.0331	0.0496
q_e (cal) (mg/g)	178.08	185.82	189.10	56.62	46.18	42.86
q_e (exp) (mg/g)	40.26	25.30	26.27	27.37	27.38	37.28
r^2	0.8939	0.9204	0.9520	0.9533	0.9672	0.9875
PSO						
k_2 (g/mg·min)	0.0033	0.0037	0.0069	0.0024	0.0027	0.0024
q_e (cal) (mg/g)	178.08	185.82	189.10	56.62	46.18	42.86
q_e (exp) (mg/g)	181.82	188.68	188.68	59.52	48.08	45.25
r^2	0.9999	0.9999	0.9998	0.9993	0.9986	0.9981
IPD						
k_{p1} (mg/g·$min^{0.5}$)	26.91	11.01	10.84	7.61	5.27	5.66
q_1 (mg/g)	64.76	132.67	136.75	12.42	10.28	2.91
r^2	0.9793	0.9900	0.9864	0.9107	0.8293	1.0000
k_{p2} (mg/g·$min^{0.5}$)	2.17	2.02	2.49	2.70	3.61	3.80
q_2 (mg/g)	158.90	167.11	167.19	31.11	15.09	12.38
r^2	0.9895	0.9968	0.9987	0.9794	0.9033	0.9095
k_{p3} (mg/g·$min^{0.5}$)	0.16	0.31	−0.43	0.17	−0.12	−0.06
q_3 (mg/g)	176.59	182.34	193.76	55.04	47.52	43.62
r^2	0.0954	0.3834	0.4119	0.2880	0.3398	0.0550

The dynamic mechanism of the MB and CR sorption process on *Rumex obtusifolius* roots is studied in three steps. The first one is film diffusion where the dye molecules move from the bulk solution to the outer surface of the adsorbent, the second one is the diffusion of the dye molecules into the pores of the adsorbent, and the last one is the adhesion of the dye molecules to the inner surface of the pores of the adsorbent [82-84]. To investigate this mechanism, the IPD kinetic model was applied to the sorption of MB and CR dyes on *Rumex obtusifolius* roots and the results shown in Fig. S4(c) and Table 5. The sorption of MB and CR dyes on *Rumex obtusifolius* roots was controlled by film diffusion, possibly followed by intraparticle diffusion, as can be seen in Fig. S4(c), and the first phase did not pass through the origin. This suggests that equilibrium was reached after the three phases were established [85,86].

7. Possible Sorption Mechanism

The possible sorption mechanism for MB and CR sorption on *Rumex obtusifolius* roots is shown in Scheme 1. As seen from the FTIR-ATR spectra in Fig. 1, it can be said that the sorption process is mediated by electrostatic interactions and hydrogen bonds with hydroxyl, carboxyl, and sulfonic functional groups on the *Rumex obtusifolius* roots surface. Since the sorption of CR dye on *Rumex obtusifolius* roots is exothermic, the H-bonds may also be effective in the binding mechanism of CR dye. In the SEM images in Fig. 3, the *Rumex obtusifolius* roots surface has a porous and fibrous structure and pore diffusion may play an active role in the sorption process. Besides, the presence of negative functional groups on the *Rumex obtusifolius* roots surface and its acidic character was supported by IGC, pH_{pzc}, and zeta potential analysis.

8. Sorption Thermodynamic Studies

To predict the mechanism and functioning of MB and CR sorption on *Rumex obtusifolius* roots, thermodynamic parameters were calculated from the equations given in Table S3 [87]. Van't Hoff plots of $\ln K_e^o$ versus 1/T for MB and CR dyes are shown in Fig. 9. The ΔH^o and ΔS^o values were calculated from the slope and intercept points of these linear plots. Then, the ΔG^o values were calculated for different temperatures using Eq. (S24) and all results listed

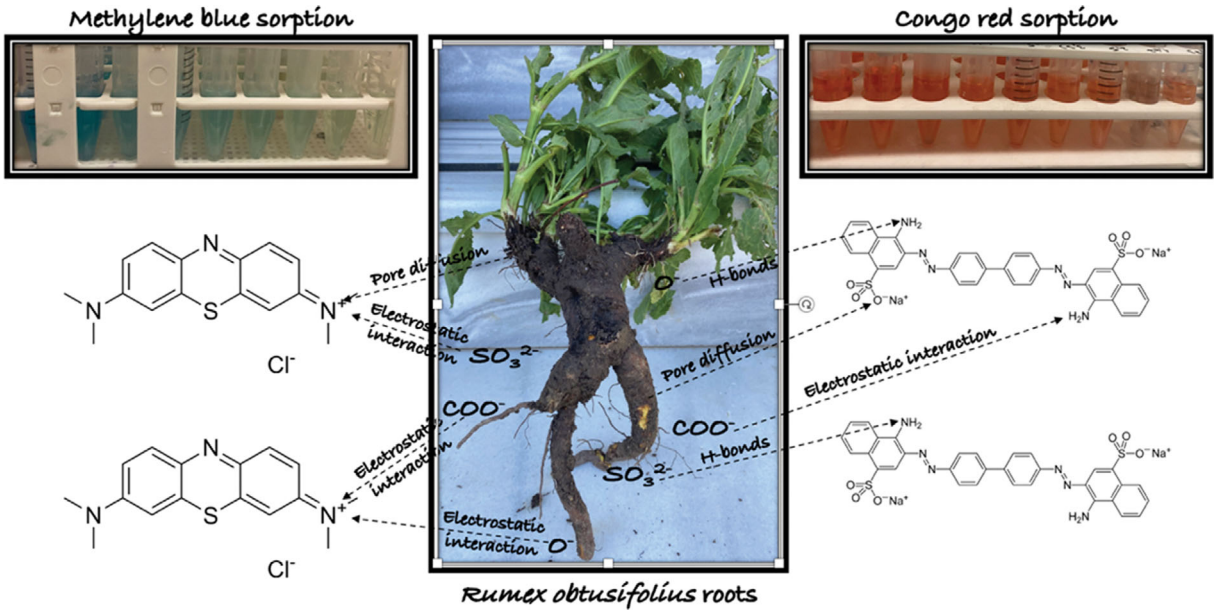

Scheme 1. Possible sorption mechanism of MB and CR dyes onto *Rumex obtusifolius* roots.

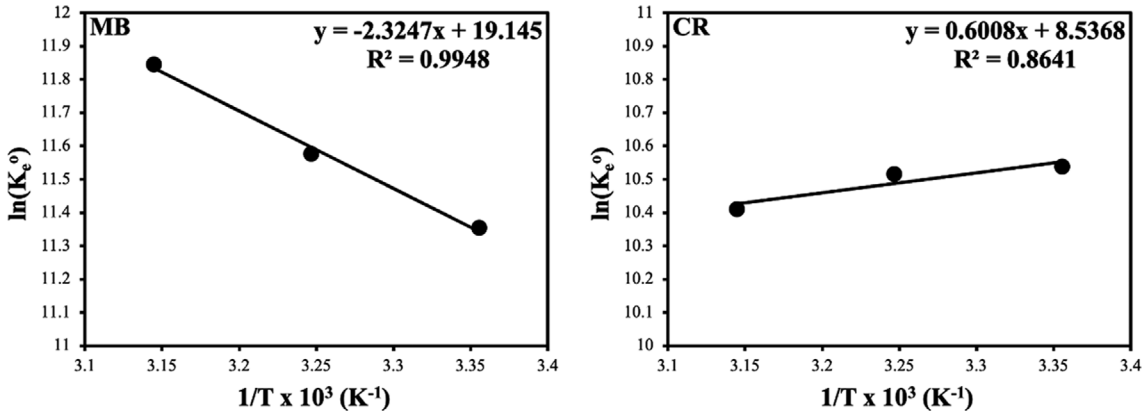

Fig. 9. The linear van't Hoff plots of MB and CR sorption onto *Rumex obtusifolius* roots.

Table 6. Thermodynamic parameters for sorption of MB and CR dyes on *Rumex obtusifolius* roots

Thermodynamic parameters	ΔH^o (kJ/mol)	ΔS^o (J/mol·K)	ΔG^o (kJ/mol)		
			298 K	308 K	318 K
MB	19.33	159.17	−28.10	−29.69	−31.28
CR	−4.99	70.97	−26.14	−26.85	−27.56

in Table 6. Positive values of ΔS^o indicate increased randomness at the solid/solution interface during the sorption of MB and CR dyes on *Rumex obtusifolius* roots and also reflect the affinity of *Rumex obtusifolius* roots for MB and CR dyes. The negative values of ΔG^o indicate that the sorption of MB and CR dyes on *Rumex obtusifolius* roots is a spontaneous process. The values of ΔG^o decrease with increasing temperature from −28.10 kJ/mol to −31.28 kJ/mol for MB dye and from −26.14 kJ/mol to −27.56 kJ/mol for CR dye, indicating that the sorption process is more spontaneous at higher temperatures. The positive value of ΔH^o for MB dye and negative value for CR dye indicate that the sorption processes are endothermic for MB dye and exothermic for CR dye. The ΔH^o values less than 40 kJ/mol for both dyes indicated that the sorption processes were physical [88,89].

CONCLUSIONS

Rumex obtusifolius roots were evaluated within the scope of zero waste and used for the effective sorption of MB and CR dyes from wastewater. *Rumex obtusifolius* roots were characterized by FTIR-ATR, SEM, BET, pH_{pzc}, and zeta potential analyses. From BET analysis, it was observed that *Rumex obtusifolius* roots had a surface area of 1.85 m^2/g and a mesoporous structure. Besides, SEM images revealed that *Rumex obtusifolius* roots have a fibrous and porous structure. From IGC studies, it was determined that their roots were acidic (K_D/K_A=0.13). From IGC, pH_{pzc}, and zeta potential results, it was predicted that *Rumex obtusifolius* roots were acidic and anionic in character and cationic pollutants would be adsorbed more effectively. In addition, the γ_S^D values were calculated from the IGC technique according to Dorris-Gray (51.10-56.68 mJ/m^2), Schultz (49.19-52.19 mJ/m^2), and Donnet-Park (49.41-54.72 mJ/m^2) approaches. It was found that the γ_S^D values increased with temperature with a more effective binding at higher temperatures. The optimum conditions for sorption were determined as pH=7, 90 min contact time, and 0.05 g/50 mL adsorbent dosage for both dyes. The effect of NaCl and $CaCl_2$ salts on the sorption process was investigated and it was observed that these ions negatively affected MB sorption while they positively affected CR sorption. The data obtained from sorption tests were applied to various isotherm models. From the high correlation coefficients, Langmuir-2 isotherm was found to be the most suitable for the sorption of both dyes, and the q_m values were calculated as 500.00 mg/g and 128.21 mg/g for MB and CR dyes at 298 K, respectively. Kinetic studies indicated that the sorption process followed the PSO kinetic. According to the IPD kinetic model, film diffusion and perhaps intraparticle diffusion was responsible for controlling the sorption of MB and CR dyes on the roots of *Rumex obtusifolius* until equilibrium was reached. From the thermodynamic parameters, it was observed that the sorption process of MB and CR dyes on *Rumex obtusifolius* roots was endothermic (ΔH^o=19.33 kJ/mol) and exothermic (ΔH^o=−4.99 kJ/mol), respectively. Also, the process was spontaneous for both dyes. From all these results, it was determined that *Rumex obtusifolius* roots can be used as an effective and eco-friendly adsorbent for the removal of various types of organic pollutants from wastewater.

SUPPORTING INFORMATION

Additional information as noted in the text. This information is available via the Internet at http://www.springer.com/chemistry/journal/11814.

REFERENCES

1. S. I. Eze, K. G. Akpomie, C. C. Ezeofor, N. V. Mmadubuike and F. K. Ojo, *Pet. Sci. Technol.*, **37**, 1830 (2019).
2. K. G. Akpomie and J. Conradie, *Environ. Chem. Lett.*, **18**, 1085 (2020).
3. D. Aksu Demirezen, D. Demirezen Yilmaz and Y. S. Yildiz, *Int. J. Biol. Macromol.*, **239**, 124311 (2023).
4. M. Akdemir, B. Isik, F. Cakar and O. Cankurtaran, *Mater. Chem. Phys.*, **291**, 126763 (2022).
5. M. Kasbaji, M. Mennani, N. Grimi, M. Oubenali, M. Mbarki, H. EL Zakhem and A. Moubarik, *Int. J. Biol. Macromol.*, **239**, 124288 (2023).
6. M. Mennani, M. Kasbaji, A. Ait Benhamou, A. Boussetta, A. A. Mekkaoui, N. Grimi and A. Moubarik, *Green Chem.*, **25**, 2896 (2023).
7. M. Radjai, H. Ferkous, Z. Jebali, H. Majdoub, R. Bourzami, G. Raffin, M. Achour, A. Gil and M. Boutahala, *J. Mol. Liq.*, **361**, 119670 (2022).
8. X. Huang, P. Hadi, R. Joshi, A. G. Alhamzani and B. S. Hsiao, *ACS Omega.*, **8**, 8634 (2023).
9. J. Abdi, M. Vossoughi, N. M. Mahmoodi and I. Alemzadeh, *Chem. Eng. J.*, **326**, 1145 (2017).
10. R. Elmoubarki, F. Z. Mahjoubi, H. Tounsadi, J. Moustadraf, M. Abdennouri, A. Zouhri, A. El Albani and N. Barka, *Water Resour. Ind.*, **9**, 16 (2015).
11. M. Loutfi, R. Mariouch, I. Mariouch, M. Belfaquir and M. S. ElYoubi, *Mater. Today Proc.*, **72**, 3638 (2023).
12. H. Ali and A. M. Ismail, *J. Polym. Environ.*, **31**, 976 (2023).
13. Y. Pi, C. Duan, Y. Zhou, S. Sun, Z. Yin, H. Zhang, C. Liu and Y. Zhao, *J. Hazard. Mater.*, **424**, 127577 (2022).
14. V. Vadivelan and K. V. Kumar, *J. Colloid Interface Sci.*, **286**, 90 (2005).
15. X. Wang, Q. Xu, L. Zhang, L. Pei, H. Xue and Z. Li, *J. Environ. Chem. Eng.*, **11**, 109206 (2023).

16. B. Isik, V. Ugraskan and O. Cankurtaran, *Sep. Sci. Technol.*, **57**, 854 (2021).
17. Z. Ahamad, M. Ahmed, F. Mashkoor and A. Nasar, *Biomass Convers. Biorefin.* (2023), https://doi.org/10.1007/s13399-023-04161-5.
18. I. Anastopoulos, A. Bhatnagar, B. H. Hameed, Y. S. Ok and M. Omirou, *J. Mol. Liq.*, **240**, 179 (2017).
19. S. Sonal, P. Prakash, B. K. Mishra and G. C. Nayak, *RSC Adv.*, **10**, 13783 (2020).
20. R. Ramaraj, A. Shanmugam, B. Nagarathinam and M. Pandi, *Biomass Convers. Biorefin.* (2023), https://doi.org/10.1007/s13399-023-04148-2.
21. S. Sismanoglu, M. K. Akalin, G. O. Akalin and F. Topak, *Bioresources*, **18**, 3414 (2023).
22. M. C. Purohit, M. Singh, G. Kumar and N. Singh, *Int. J. Pharm. Sci. Res.*, **11**, 4524 (2020).
23. D. Harshaw, L. Nahar, B. Vadla, G. Saif-E-Naser and S. Sarker, *Arch. Biol. Sci.*, **62**, 387 (2010).
24. khalid S. Alshallash, *Biologia*, **76**, 33 (2021).
25. B. Isik, S. Avci, F. Cakar and O. Cankurtaran, *Environ. Sci. Pollut. Res.*, **30**, 1333 (2023).
26. N. Cordeiro, C. Gouveia, A. G. O. Moraes and S. C. Amico, *Carbohydr. Polym.*, **84**, 110 (2011).
27. S. Bensalem, B. Hamdi, S. Del Confetto, M. Iguer-Ouada, A. Chamayou, H. Balard and R. Calvet, *Colloids Surf. A Physicochem. Eng. Asp.*, **516**, 336 (2017).
28. F. Cakar, H. Ocak, E. Ozturk, S. Mutlu-Yanic, D. Kaya, N. San, O. Cankurtaran, B. Bilgin-Eran and F. Karaman, *Liq. Cryst.*, **41**, 1323 (2014).
29. I. Erol, F. Cakar, H. Ocak, H. Cankurtaran, O. Cankurtaran, B. Bilgin-Eran and F. Karaman, *Liq. Cryst.*, **43**, 142 (2016).
30. H. Wang, L. Yang, Y. Qin, Z. Chen, T. Wang, W. Sun and C. Wang, *Colloids Surf. A Physicochem. Eng. Asp.*, **656**, 130290 (2023).
31. A. Mohrazi and R. Ghasemi-Fasaei, *Environ. Monit. Assess.*, **195**, 339 (2023).
32. S. C. Karadeniz, B. Isik, V. Ugraskan and F. Cakar, *Phys. Chem. Earth, Parts A/B/C.*, **129**, 103338 (2023).
33. Z. M. Senol, S. Cetinkaya and H. Arslanoglu, *Biomass Convers. Bioref.*, **13**, 2413 (2023).
34. K. S. W. Sing, *Pure Appl. Chem.*, **57**, 603 (1985).
35. Z. Wang, X. Jiang, M. Pan and Y. Shi, *Minerals*, **10**, 377 (2020).
36. K. Jasri, A. S. Abdulhameed, A. H. Jawad, Z. A. ALOthman, T. A. Yousef and O. K. Al Duaij, *Diam. Relat. Mater.*, **131**, 109581 (2023).
37. R. Foroutan, S. J. Peighambardoust, P. Latifi, A. Ahmadi, M. Alizadeh and B. Ramavandi, *J. Environ. Chem. Eng.*, **9**, 106344 (2021).
38. K. Ito and J. E. Guillet, *Macromolecules*, **12**, 1163 (1979).
39. A. U. Itodo, H. U. Itodo and M. K. Gafar, *J. Appl. Sci. Environ. Manage.*, **14**, 141 (2010).
40. M. Kasbaji, M. Mennani, A. Boussetta, N. Grimi, F. J. Barba, M. Mbarki and A. Moubarik, *Sep. Sci. Technol.*, **58**, 221 (2023).
41. A. Dbik, S. Bentahar, M. El Khomri, N. El Messaoudi and A. Lacherai, *Mater. Today Proc.*, **22**, 134 (2020).
42. P. K. Rose, R. Kumar, R. Kumar, M. Kumar and P. Sharma, *Groundw. Sustain. Dev.*, **21**, 100931 (2023).
43. A. H. Jawad, S. E. M. Saber, A. S. Abdulhameed, A. M. Farhan, Z. A. ALOthman and L. D. Wilson, *J. King Saud. Univ. Sci.*, **35**, 102630 (2023).
44. B. Isik, V. Ugraskan, F. Cakar and O. Yazici, *Res. Chem. Intermed.*, **48**, 4249 (2022).
45. B. Isik, F. Cakar, O. Cankurtaran and H. Cankurtaran, *ChemistrySelect.*, **6**, 6740 (2021).
46. A. Legras, A. Kondor, M. Alcock, M. T. Heitzmann and R. W. Truss, *Cellulose*, **24**, 4691 (2017).
47. M. L. Palash, A. Pal, T. H. Rupam, B. D. Park and B. B. Saha, *Colloids Surf. A Physicochem. Eng. Asp.*, **603**, 125209 (2020).
48. A. C. Adiguzel, B. Korkmaz, F. Cakar, B. F. Senkal and O. Cankurtaran, *Turk. J. Chem.*, **45**, 1533 (2021).
49. H. Ocak, O. Yazici, B. Bilgin Eran, O. Cankurtaran and F. Karaman, *Optoelectron. Adv. Mater. Rapid Commun.*, **2**, 303 (2008).
50. V. Swaminathan, J. Cobb and I. Saracovan, *Int. J. Pharm.*, **312**, 158 (2006).
51. V. Ugraskan, B. Isik, O. Yazici and F. Cakar, *Solid State Sci.*, **118**, 106636 (2021).
52. Y. Xu, J. Lin, J. Xia and B. Hu, *Chin. J. Chromatogr.*, **29**, 249 (2011).
53. V. Gutmann, *The donor-acceptor approach to molecular interactions*, Plenum, New York (1978).
54. K. Yadav, S. R. Latelwar, D. Datta and B. Jana, *J. Ind. Chem. Soc.*, **100**, 100974 (2023).
55. D. M. N. H. Jayasuriya and K. Nadarajah, *Water Sci. Eng.*, **16**, 154 (2023).
56. K. Akin, V. Ugraskan, B. Isik and F. Cakar, *Int. J. Biol. Macromol.*, **223**, 543 (2022).
57. M. A. Abdelaziz, M. E. Owda, R. E. Abouzeid, O. Alaysuy and El. I. Mohamed, *Int. J. Biol. Macromol.*, **225**, 1462 (2023).
58. P. K. Rose, R. Kumar, R. Kumar, M. Kumar and P. Sharma, *Groundw. Sustain. Dev.*, **21**, 100931 (2023).
59. M. Bilgi, V. Ugraskan and B. Isik, *Chem. Eng. Commun.*, **210**, 1405 (2022).
60. A. H. Jawad, R. A. Rashid, M. A. M. Ishak and K. Ismail, *J. Taibah Univ. Sci.*, **12**, 809 (2018).
61. A. H. Jawad, R. Razuan, J. N. Appaturi and L. D. Wilson, *Surf. Interface*, **16**, 76 (2019).
62. H. Duran, S. Sismanoglu and T. Sismanoglu, *J. Ind. Chem. Soc.*, **96**, 1245 (2019).
63. Y. Tang, M. Li, C. Mu, J. Zhou and B. Shi, *Chemosphere*, **229**, 570 (2019).
64. H. Munjur, N. Hasan, R. Awual, M. Islam, M. A. Shenashen and J. Iqbal, *J. Mol. Liq.*, **319**, 114356 (2020).
65. S. Joshi, V. K. Garg, N. Kataria and K. Kadirvelu, *Chemosphere*, **236**, 124280 (2019).
66. S. Pandey, J. Y. Do, J. Kim and M. Kang, *Int. J. Biol. Macromol.*, **143**, 60 (2020).
67. E. Alver, A. U. Metin and F. Brouers, *Int. J. Biol. Macromol.*, **154**, 104 (2020).
68. Mu. Naushad, A. A. Alqadami, A. A. Al-Kahtani, T. Ahamad, R. Awual and T. Tatarchuk, *J. Mol. Liq.*, **296**, 112075 (2019).
69. W. Xiao, Z. N. Garba, S. Sun, I. Lawan, L. Wang, M. Lin and Z. Yuan, *J. Clean. Prod.*, **253**, 119989 (2020).
70. S. Sultana, K. Islam, A. Hasan, H. M. J. Khan, M. A. R. Khan, A. Deb, Al Raihan and W. Rahman, *Environ. Nanotechnol. Monit. Manag.*, **17**, 100651 (2022).
71. K. C. Nebaghe, Y. El Boundati, K. Ziat, A. Naji, L. Rghioui and M. Saidi, *Fluid Phase Equilib.*, **430**, 188 (2016).

72. R. Temiz, B. Isik, V. Ugraskan and O. Cankurtaran, *Biomass Convers. Biorefin.* (2022), https://doi.org/10.1007/s13399-022-03680-x.
73. S. Shakoor and A. Nasar, *J. Taiwan Inst. Chem. Eng.*, **66**, 154 (2016).
74. R. Ahmad Aftab, S. Zaidi, A. Aslam Parwaz Khan, M. Arish Usman, A. Y. Khan, M. Tariq Saeed Chani and A. M. Asiri, *Alexandria Eng. J.*, **71**, 355 (2023).
75. Z. Li, H. Hanafy, L. Zhang, L. Sellaoui, M. Schadeck Netto, M. L. S. Oliveira, M. K. Seliem, G. Luiz Dotto, A. Bonilla-Petriciolet and Q. Li, *Chem. Eng. J.*, **388**, 124263 (2020).
76. P. Ganguly, R. Sarkhel and P. Das, *Surf. Interface*, **20**, 100616 (2020).
77. H. Freundlich, *J. Phys. Chem.*, **57**, 385 (1906).
78. A. Bukhari, T. Javed and M. N. Haider, *J. Dispers. Sci. Technol.*, (2022).
79. S. Kaur, S. Rani and R. K. Mahajan, *Desalin. Water Treat.*, **53**, 1957 (2015).
80. S. Karakus, S. Sismanoglu, G. Akdut, O. Urk, E. Tan, T. Sismanoglu and A. Kilislioglu, *J. Chem. Soc. Pak.*, **39**, 17 (2017).
81. A. salah omer, G. A. El Naeem, A. I. Abd-Elhamid, O. O. M. Farahat, A. A. El-Bardan, H. M. A. Soliman and A. A. Nayl, *J. Mater. Res. Technol.*, **19**, 3241 (2022).
82. Z. M. Senol, S. Cetinkaya, A. F. Yenidunya, F. Basoglu-Unal and A. Ece, *Int. J. Biol. Macromol.*, **199**, 318 (2022).
83. A. M. Al-Ma'abreh, R. A. Abuassaf, D. A. Hmedat, M. Alkhabbas, G. Edris, S. H. Hussein-Al-Ali and S. Alawaideh, *Int. J. Mol. Sci.*, **23**, 11959 (2022).
84. M. Saxena, N. Sharma and R. Saxena, *Surf. Interface*, **21**, 100639 (2020).
85. R. A. Fideles, G. M. D. Ferreira, F. S. Teodoro, O. F. H. Adarme, L. H. M. da Silva, L. F. Gil and L. V. A. Gurgel, *J. Colloid Interface Sci.*, **515**, 172 (2018).
86. Z. Wang, S. Bin Kang and S. W. Won, *Colloids Surf. A Physicochem. Eng. Asp.*, **647**, 128983 (2022).
87. E. C. Lima, A. Hosseini-Bandegharaei, J. C. Moreno-Piraján and I. Anastopoulos, *J. Mol. Liq.*, **273**, 425 (2019).
88. D. Ozdes, A. Gundogdu, C. Duran and H. B. Senturk, *Sep. Sci. Technol.*, **45**, 2076 (2010).
89. W. Qu, T. Yuan, G. Yin, S. Xu, Q. Zhang and H. Su, *Fuel*, **249**, 45 (2019).